

Adsorption of Small Hydrocarbons on the Three-Fold PdGa Surfaces: The Road to Selective Hydrogenation

Jan Prinz,*^{II} Carlo A. Pignedoli,^{II} Quirin S. Stöckl,[†] Marc Armbrüster,[‡] Harald Brune,[§] Oliver Gröning,^{II} Roland Widmer, and Daniele Passerone*^{II}

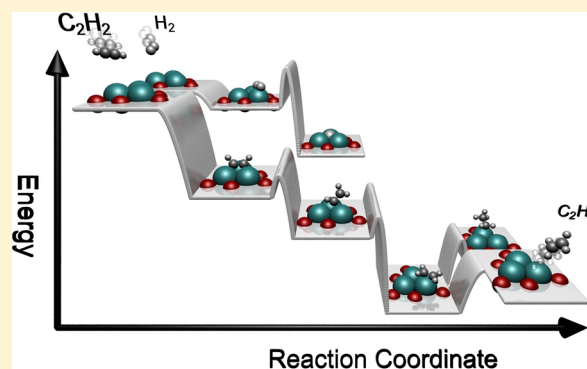
^{II}Nanotech@surfaces Laboratory and [†]Nanoscale Materials Science, Empa. Swiss Federal Laboratories for Materials Science and Technology, Ueberlandstrasse 129, 8600 Dübendorf, Switzerland

[‡]Max-Planck-Institut für Chemische Physik fester Stoffe, 01187 Dresden, Germany

[§]Institute of Condensed Matter Physics, Ecole Polytechnique Fédérale de Lausanne (EPFL), Station 3, 1015 Lausanne, Switzerland

W Web-Enhanced Feature S Supporting Information

ABSTRACT: Intermetallic compounds are a promising class of materials as stable and selective heterogeneous catalysts. Here, the (111) and ($-1-1-1$) single crystal surfaces of the PdGa intermetallic compound were studied as model catalysts with regard to the selective hydrogenation of acetylene (C_2H_2) to ethylene (C_2H_4). The distinct atomic surface structures exhibit isolated active centers of single atomic and three atomic Pd ensembles, respectively. For the two prototypal model catalyst surfaces, the adsorption sites and configurations for hydrogen (H_2), acetylene, and ethylene were investigated by combining scanning tunneling microscopy, temperature-programmed desorption, and *ab initio* modeling. The topmost Pd surface atoms provide the preferred adsorption sites for all studied molecules. The structural difference of the Pd ensembles has a significant influence on the adsorption energy and configuration of C_2H_2 , while the influence of the ensemble structure is weak for C_2H_4 and H_2 adsorption. To approach the question of catalytic performance, we simulated the reaction pathways for the heterogeneous catalytic hydrogenation of acetylene on the two surfaces by means of density functional theory. Due to the geometrical separation of the Pd sites on the surfaces, the steric approach of the reactants (H and C_2H_x) was found to be of importance to the energetics of the reaction. The presented study gives a direct comparison of binding properties of catalytic Pd on-top sites vs three-fold Pd hollow sites and is therefore of major relevance to the knowledge-based design of highly selective hydrogenation catalysts.



1. INTRODUCTION

Selective hydrogenations are a class of reactions essential in many pharmaceutical and petrochemical processes. It is of particular importance in the industrial production of polyethylene, where the removal of acetylene from the ethylene feedstock is pivotal to prevent poisoning of the polymerization catalyst.¹ The most efficient way to accomplish this purification is to convert the contaminant into the valuable reactant through catalytic semihydrogenation.² The “optimal” heterogeneous catalyst in this case maintains the same properties during the reaction (stability), enhances the transformation to ethylene (activity), and hinders further reaction to unwanted products like ethane or heavier hydrocarbon species (selectivity). The replacement of the primarily applied oxide supported pure Pd catalyst by bimetallic Pd–Ag alloys has yielded a significant increase in selectivity for this reaction.^{2,3} The increased selectivity is assigned to the formation of small, catalytically active Pd ensembles, embedded in the matrix of less active Ag. The separated ensembles of only a few atoms offer a reduced number of adsorption conformations for reactants and

consequently increase selectivity by reducing the number of possible reaction pathways, which is known as the ensemble effect.⁴ Indeed, it was found that bimetallic catalysts often exhibit different reaction selectivity than their catalytically active monometallic constituents.⁵

In this respect, intermetallic compounds (IMC) have obtained increasing attention in the field of catalysis research, as the distinct crystal structure leads to well-defined surfaces that might exhibit small separated ensembles of active metal atoms with high areal density. They therefore offer the possibility to combine high catalytic selectivity with high activity.^{6–8} In recent experiments, PdGa IMCs were shown to be highly selective catalysts in the semihydrogenation of acetylene.^{3,9} While Pd is assumed to play the major role in the catalytic reaction, Ga is considered as the atomic spacer in between the active Pd sites. The crystal structure of PdGa exhibits a shell of 7 Ga atoms as nearest neighbors to each Pd

Received: June 13, 2014

Published: July 28, 2014

atom and consequently the Pd atoms are spatially separated from each other.^{9,10} However, the question remains if, and to which extent, the bulk Pd separation leads to separated Pd reaction centers at the catalysts surfaces. As the catalytic experiments,^{3,9} evidencing high activity and selectivity, were performed on polycrystalline samples, the favorable catalytic properties cannot be unambiguously related to specific atomic surface structures, i.e., to the ensemble effect.

To gain more insight, we recently studied the atomic structures and the adsorption of CO on the three-fold surfaces of the PdGa IMC.^{11,12} Here, we investigate the two polar (111) and ($-1-1-1$) terminations, exhibiting trimers of Pd atoms (Pd_3) and single atoms (Pd_1) on the outermost layers, respectively, with regard to the ensemble effect in the semihydrogenation of acetylene. We focus on the determination of the adsorption sites and configurations for hydrogen, acetylene, and ethylene by means of scanning tunneling microscopy (STM) and density functional theory (DFT). We then propose a theoretical model for the catalytic reaction pathway toward ethylene and compare the mechanism for successive hydrogens of acetylene on the two surfaces, focusing on barrier heights and binding energies for the reaction intermediates.

2. METHODS

Details on crystal growth and UHV surface preparation and can be found in refs 10, 11, and 13. C_2H_2 (purity 99.6%) from a solvent free container was cleaned by freeze–thaw cycling (77 K) before dosing. C_2H_4 and H_2 of purity 99.996% (CANGAS) were used without precleaning. All gases were dosed by chamber backfilling through a leak valve. Effective exposure was achieved by removing the sample from the cold STM stage for a short time (20 s), which might lead to a slightly increased temperature during adsorption.

STM measurements were conducted using an Omicron low-temperature STM at a base pressure below 5×10^{-11} mbar and an etched Pt/Ir tip.

Computational parameters and methods were described in earlier publications.^{12,14,15} The well-established PBE parametrization was used for the DFT exchange correlation functional.¹⁵ Reaction barriers were computed using the nudged elastic band (NEB) method (see Supporting Information (SI) for further details).¹⁶

3. DETERMINATION OF ADSORPTION SITES

As a first step to answer the question of how the atomic surface structure of PdGa is influencing the catalytic semihydrogenation of acetylene, we identify the favored adsorption sites of the reactants and of the product. To this end, we performed low-temperature STM measurements on the three-fold PdGa surfaces after exposure to hydrogen, acetylene, and ethylene, respectively. The molecules were dosed on the cold surfaces (5 K for C_2H_2 and H_2 to reduce molecular motion and enable adsorption, respectively; 77 K for C_2H_4) by backfilling of the chamber. Submonolayer coverages were achieved after an exposure of the surfaces to about 0.05 L for all molecules. Figure 1 shows STM images of the PdGa:A($-1-1-1$) Pd_3 (abbreviated as Pd_3) and PdGa:A(111) Pd_1 (Pd_1) surfaces after exposure to molecular hydrogen at 5 K.

The atomic structures of the clean substrates have been determined and discussed in an earlier publication¹¹ and are superimposed as ball models in the insets. While the top layer of the Pd_3 termination exhibits one trimer of Pd atoms per unit cell, the Pd_1 termination exhibits only one isolated Pd atom per unit cell. In both cases these Pd ensembles are well separated from their nearest Pd neighbors and arranged in a hexagonal

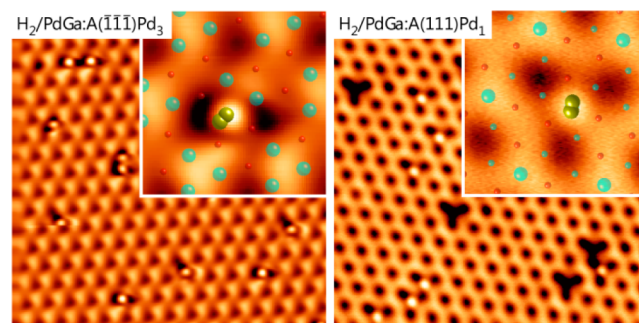


Figure 1. STM images (10×10 nm) of H_2 adsorbed at $T = 5$ K on PdGa:A($-1-1-1$) Pd_3 (left) and on PdGa:A(111) Pd_1 (right). The hexagonal periodicity of the topmost atomic layers of the two three-fold surfaces is visible. Insets show a magnified section (1.5×1.5 nm) of a single molecule. The superimposed atomic ball models show the lowest energy adsorption configurations as determined by DFT (Pd: cyan, Ga: red, H: yellow). For clarity, the atoms of the terminating layers and H are drawn with enlarged radii. In the right panel, the surface vacancy defects typical for the Pd_1 termination¹¹ appear as dark, three-fold features. (Tunneling parameters: left: -5 mV, 1 nA; right: 5 mV, 20 pA).

pattern with a lattice constant of 0.69 nm (see also ball models in Figure 2). In STM, the Pd atoms appear as bright

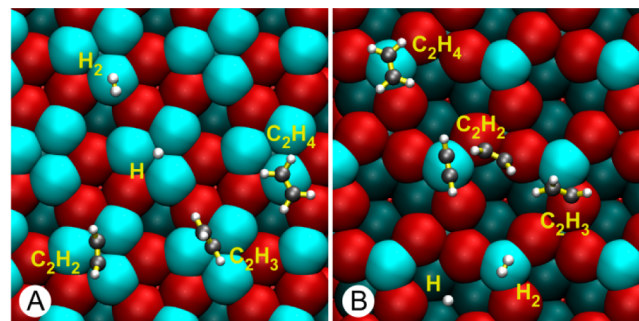


Figure 2. Summary of the DFT optimized, minimum energy adsorption configurations for various molecules on the Pd_3 (A) and the Pd_1 (B) surfaces, respectively. (Pd: cyan, Pd(subsurface): dark cyan, Ga: red, C: black). Most adsorption sites are located on the topmost Pd atoms.

protrusions on the two surfaces.¹¹ In the STM images of Figure 1, single H_2 molecules can easily be distinguished, and their adsorption position within the unit cell is identified from the superposition with the atomic structure. For both surfaces, the application of tunneling voltages larger than about 100 mV leads to immediate desorption of all adsorbates in the vicinity of the tip. This, and the fact that deposition at 77 K is not possible, indicates a rather weak physisorption of the adsorbate on the surface.

On Pd_3 , the H_2 molecules appear off center with respect to the protrusions marking the Pd trimer centers. Furthermore, three symmetrically equivalent such off-center sites are found. Upon applying higher tunnel voltages, transitions from one position to another are observed as well as hopping to neighboring surface unit cells. A series of images of the tip-induced hopping of the molecules is shown in the SI. Also two hydrogen molecules are occasionally observed on the same Pd trimer. From the off-center appearance and the overlay with the DFT optimized structure we identify the H_2/Pd_3 adsorption position as an on-top site of one Pd atom of the trimer.

In the right-hand panel of Figure 1, the molecules appear as a bright protrusion centered on the isolated Pd atoms of the Pd_1 termination. Other adsorption sites were not observed. Also on this surface, molecular hopping can be triggered by scanning with higher voltages or by applying voltage pulses (≈ 90 mV) to the tunnel junction close to the molecules.

To achieve a more detailed understanding of the adsorption properties, we used DFT to compute the energetically most stable adsorption sites for the relevant molecules. The resulting configurations are summarized for Pd_3 and Pd_1 in the left- and right-hand panels of Figure 2, respectively.

The DFT results for the molecular hydrogen adsorption are in agreement with the observations from the STM experiments. For H_2 on Pd_3 and Pd_1 , the energetically most favored sites are on top of the Pd atoms of the topmost layer in both cases, with an average Pd–H distance of 1.90 pm Å and the H–H molecular axis almost parallel to the surface plane.¹¹ The binding energies are small, with -0.25 eV (Pd_3) and -0.29 eV (Pd_1). For Pd_3 , the molecule binds slightly off-center on one of the Pd atoms of the trimer, with the molecular axis pointing away from the trimer center. For the case of atomic hydrogen, the energetically favored adsorption positions are the three-fold hollow site of the Pd trimer for Pd_3 and the three-fold hollow site of the subsurface Pd trimer for Pd_1 . The positions of the features seen by STM clearly coincide with the theoretically favored position of the H_2 and not with that of the H adsorption site. Therefore, we find that H_2 dissociation does not occur at 5 K, which is further supported by the tip-induced desorption at low tunnel voltages of >90 mV. Furthermore, it is noteworthy that H_2 behaves differently than CO regarding adsorption on the Pd trimer on Pd_3 . For H_2 only Pd on-top site adsorption is present for Pd_3 and Pd_1 , while for CO the Pd_3 trimers allow for hollow site adsorption at low coverages.¹² This might well be due to the upstanding adsorption configuration of the dipolar CO molecule, while the two H atoms in H_2 are identically charged, and thus the molecule prefers a flat lying orientation.

Figure 3 shows STM images of adsorbed C_2H_2 molecules on the two three-fold PdGa surfaces. As in the H_2 case, acetylene is found to bind preferably to the Pd centers of the topmost layer. Single molecules are easily distinguishable, however, their STM topographies are very different on the two surfaces. While on Pd_3 , a single molecule appears as two protruding lobes, a single, almost circular feature is seen on Pd_1 .

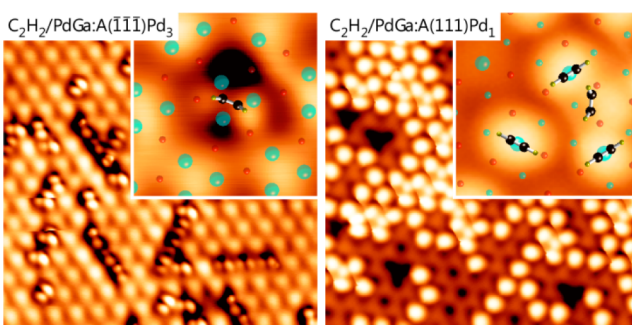


Figure 3. STM images (10×10 nm) of acetylene (C_2H_2) adsorbed at $T = 5$ K on Pd_3 (left) and Pd_1 (right). While in the former case, the molecules have a two-lobed appearance, a round shape is found in the latter. For C_2H_2/Pd_1 (right panel), two different adsorption sites are occupied. (Tunneling parameters: left: 5 mV, 50 pA; right: 5 mV, 10 pA).

For C_2H_2/Pd_3 we find three symmetrically equivalent orientations of the molecule that are characterized by 120° rotations of the two-lobe feature around the center of the Pd trimer. Transitions between these orientations can be induced by increasing the tunneling voltage, ultimately leading to a three-fold symmetric shape for $V_T > 0.2$ V, since the frequency of the rotation can no longer be resolved by STM, as shown in Figure 4. Analysis of the transition frequency as a function of

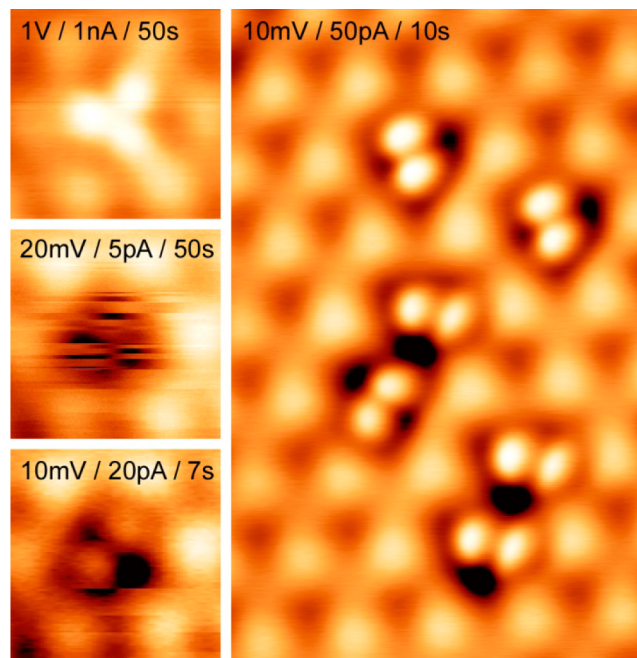


Figure 4. STM appearance of C_2H_2 adsorbed on $PdGa:A(-1-1-1)Pd_3$ strongly depends on the applied tunneling conditions. Values given in each panel are tunnel voltage/tunnel current/approximate time to scan the molecule. In the top left panel, the electron-induced molecular rotation between the three states is too fast to be resolved by the STM, leading to a three-fold appearance. To resolve the molecular orientation, a low tunneling voltage and current (middle and bottom panel) and a fast scan speed (bottom and right panel) have to be chosen. In the right panel, the three symmetrically equivalent molecular orientations are identified.

gap voltage yields a barrier of 32 meV for the rotation, but even for lower gap voltages infrequent rotation is observed. Occasionally, a correlated alignment of the rotational state between neighboring adsorbates is detected (see Figure 3), leaving the molecules slightly more stable against tip-induced rotation. This can be seen in the STM video, which is available in the online version of the article. Accordingly, full site isolation is not established for C_2H_2 adsorbed the Pd_3 trimers, as molecular orientations are not completely independent. The weak collective arrangement can be disturbed by increasing the tunneling voltage but is partially reestablished after recording of a few images with reduced voltages. In the Supporting Information, a series of images illustrates the distortion and rearrangement of adsorbed C_2H_2 on Pd_3 . Similar electron-induced rotation has been reported for C_2H_2 on $Pd(111)$.¹⁷ However, in contrast to the close-packed single element metal surface, the site separation on the intermetallic PdGa surface does not allow for tip-induced diffusion of C_2H_2 molecules to a neighboring Pd_3 site, since hopping was never observed for the applied tunneling conditions ($V_T \leq 2$ V, $I_T \leq 10$ nA).

The superposition of the DFT computed adsorption geometry and the STM topography in the inset of the left panel in Figure 3 reveals excellent agreement between theory and experiment. The comparison shows that the two bright lobes are located at the positions of the hydrogen atoms of the acetylene molecule, which is adsorbed on the Pd trimer in a slightly asymmetric π /di- σ bonding configuration,¹⁸ as found by DFT. Each of the two carbon atoms forms a σ -bond to one atom of the Pd trimer, and the π orbital of the molecule forms a bond to the third Pd atom of the trimer, leading to a tilt of the C–H bonds and a shift of the C–C axis toward the center of the trimer. The two H–C–C bond angles are 130.5° and 128.5°, indicating that the hybridization of the C atoms has changed from sp to sp². The C–C triple bond, typical of the gas phase, is reduced to a double bond (signaled by an increase of the bond length from 121 to 134 pm), resulting in an overall adsorption energy of −1.17 eV. While the bonding geometry is comparable to literature data of C₂H₂ on Pd(111), the binding energy is significantly larger on the single element surface (−1.78 eV).^{19,20}

For C₂H₂/Pd₁, the STM image in the right panel of Figure 3 reveals the existence of two different adsorption sites. The most abundant site is on the topmost Pd₁ atom. Less frequently observed is the adsorption in the center of three occupied on-top Pd sites, on top of Ga atoms. Please note that the surface atomic structures shown in all figure insets are well-defined, and their angular orientations are carefully matched with the structure determination by low-energy electron diffraction (LEED-I(V)).¹¹ Hence, we find the alternative site for C₂H₂/Pd₁ located on the Ga trimer of the second atomic layer, as can be seen from the superposition of the atomic surface structure (see right inset in Figure 3). The comparison to the DFT relaxed atomic structure of the single molecule, i.e., without the neighboring Pd on-top sites occupied, does not yield full agreement with the STM image as DFT suggests an off-center adsorption. However, we cannot exclude that the round shapes of the molecules on C₂H₂/Pd₁, as seen by STM, are due to fast rotation, or hopping, between iso-energetic configurations.

In order to achieve stable imaging for C₂H₂/Pd₁, such as in Figure 3, it is necessary to reduce the tunnel current to about 10 pA. After continuously imaging an area with increased tunnel current (\approx 50 pA), some of the interstitial adsorbates disappear and reappear at an unoccupied on-top Pd site in the vicinity, confirming that the two observed features are of the same molecular species (for details see SI). We found that the adsorption energies computed by DFT for C₂H₂ in the two different adsorption sites of Pd₁ are similar, in agreement with the fact that both types are observed in experiment. The experimental observation that adsorbates can be transferred more easily from the interstitial to the Pd top site than the other way around suggests that the latter is slightly more stable. In the on-top Pd site, C₂H₂ is π -bonded and has an adsorption energy of −0.61 eV with angles of 162° for both C–C–H bonds. The interstitial adsorption configuration is π /di- σ bonded to two Ga atoms of the second and one Pd atom of the third layer (Figure 2B), yielding an almost equivalent adsorption energy of 0.60 eV with C–C–H bond angles of 122° and 123° for the two H.

The different bonding characters of acetylene in the different π or σ bonding configurations on the two surfaces are reflected in the DFT computed C–C bonding distances of 124 pm for π -bonded C₂H₂ on the outermost Pd atoms of Pd₁; 135 pm for the σ -bond to the second layer Ga atoms on Pd₁; and 134 pm

for the σ -bond to the Pd₃ trimers (for comparison: 121 pm in the gas phase). Other possible adsorption sites were found to have considerably lower adsorption energies. The significant binding energy difference of acetylene bound to Pd₃ (−1.17 eV) and Pd₁ (−0.61 eV) is noteworthy, particularly in view that this difference occurs for two opposed surfaces of the same crystal. The origin of this effect lies in the size and configuration of the topmost atomic Pd ensembles on the two surfaces, as their electronic structures are almost identical.¹¹ Hence, as presented earlier for CO¹², we observe a strong ensemble effect for C₂H₂ adsorbed on the three-fold intermetallic PdGa surfaces.

Finally, we turn our attention to the product of the acetylene semihydrogenation, i.e. ethylene C₂H₄. STM images after adsorption at 77 K are shown in Figure 5. On Pd₃ the

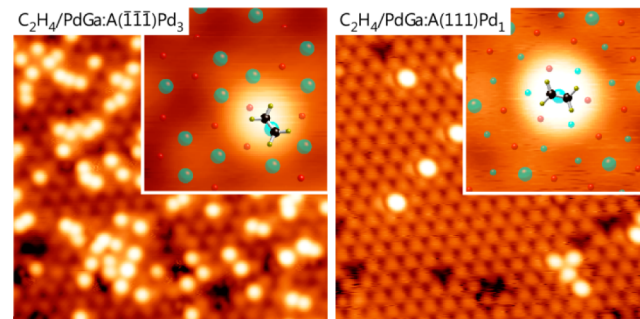


Figure 5. STM images (10 × 10 nm) of ethylene (C₂H₄) adsorbed at T = 77 K on Pd₃ (left) and Pd₁ (right). The molecules appear as round protrusions on both surfaces. On Pd₁, the features are found on top of the isolated Pd atoms, while on Pd₃, they show a lateral offset with respect to the Pd trimer centers. The inset for Pd₃ reveals that the features coincide with the positions of one of the Pd atoms in the trimer. Dark areas in the bottom of the left panel are due to contaminants. Tunneling parameters: left: −100 mV, 100 pA; right: −175 mV, 200 pA.

molecules are off-center with respect to the Pd trimer and almost on top of a single Pd atom of the Pd trimer. This is in agreement with the energetically favored configuration found by DFT, as shown in the left inset in Figure 5. The binding energy amounts to −0.69 eV, with a C–C bond distance of 138 pm and with the C–C axis slightly tilted by 6° with respect to the surface plane (see Figure 2A). In STM we see evidence for some of the trimers being occupied by two molecules, with each appearing as a protrusion almost on top of the single Pd atoms of the trimer (see SI). Calculations show that if two C₂H₄ are placed on the same trimer, they repel each other, yielding a reduced total binding energy of −0.50 eV per molecule. The occurrence of three C₂H₄ per trimer was never observed in STM, which indicates a limitation of the total coverage due to steric hindrance.

For the adsorption of C₂H₄ on Pd₁, STM reveals round protrusions, centered on the single Pd atoms of the topmost layer. This configuration is very similar to the one of acetylene on this surface described above. However, also for higher coverages of ethylene (not shown), interstitial adsorbates are not seen in our experiments. DFT yields a binding energy of −0.73 eV for the case of C₂H₄ in a π -bonded conformation on top of the Pd atoms, with the C–C axis parallel to the surface plane and a slight distortion of the C–C–H bonds to 168°. Notably, in both studied cases of C₂H₄ on Pd₃ and Pd₁, the bonding configurations are different from that on the clean

Pd(111) surface, where C_2H_4 is reported to adsorb preferably in a di- σ bridge position between two neighboring Pd atoms, yielding a binding energy of -0.64 eV.²¹

In Table 1, adsorption energies for hydrocarbons and hydrogen are summarized. The overview of the energetically

Table 1. Adsorption Energies in eV Determined by DFT for Some of the Adsorbed Species Presented in Figure 2

	Pd ₃	Pd ₁
H ₂	-0.25	-0.29
H + H	-1.01	-0.51
C ₂ H ₂	-1.17	-0.61 ^a (-0.60) ^b
C ₂ H ₄	-0.69	-0.73

^aOn-top Pd. ^bOn Ga trimer.

most favorable bonding sites shown in Figure 2 reveals that on Pd₃, molecules and reaction intermediates (discussed later in the text) bind preferentially to the Pd trimers. On Pd₁, also bonding to Ga atoms is observed for some cases (alternative site for C₂H₂ and C₂H₃), which was not indicated by the adsorption of CO used as a test molecule in an earlier study.¹² Remarkably, a recent DFT study revealed that also on PdGa(210) C₂H₂ and C₂H₃ bind preferentially with at least one σ bond to a Ga atom of the surface.²² As the electronic structures of the Pd₁, Pd₃, and PdGa(210) surfaces are approximately equivalent,¹¹ this effect is ascribed to the geometrical arrangements of the surface atoms, which are rather open structures for Pd₁ and PdGa(210) but rather dense in the Pd₃ case. Accordingly, the Pd₃ termination seems to provide a special case, in which the Pd trimers of the topmost layer are packed dense enough to prevent the bond of the hydrocarbons to the second layer of Ga atoms.

To test the accuracy of the computed binding energies given above, we performed temperature-programmed desorption (TPD) for acetylene, which yielded the largest differences in binding energy between the two surfaces. The desorption curves are presented in Figure 6.

The peak positions in the TPD data confirm the DFT result that Pd₃ binds C₂H₂ significantly stronger than Pd₁. Assuming first-order desorption, we derive a binding energy ratio of 1.5 from the two desorption temperatures. From simulation of the desorption process based on the theory by Redhead²³ (first-

order, desorption attempt frequency: 1×10^{13} Hz, ramp: 6 K/s), we find desorption energies of 0.52 and 0.80 eV for C₂H₂ on Pd₁ and Pd₃. While in the first case, agreement with DFT is acceptable (DFT: 0.61 eV), the desorption energy in the latter case is with 0.8 eV smaller in experiment than in theory (DFT: 1.17 eV). This might be due to different desorption attempt frequencies for acetylene bound in a π /di- σ , or a π configuration, leading to a peak-shift in the experiment. However, we cannot exclude that the discrepancy is caused by an overestimation of the σ bond to the Pd₃ trimers by the DFT method. Nevertheless, the ratio of the desorption temperatures on the two surfaces of 1.54 is in reasonably good agreement with the ratio of the DFT computed adsorption energies of 1.92. The increase of the background signal with temperature in Figure 6 is assigned to desorption from the sample holder.

4. DFT STUDY ON THE SEMIHYDROGENATION OF ACETYLENE

To address the performance of the two model catalysts we extend the theoretical analysis toward the reaction pathway of the semihydrogenation of acetylene. The very good agreement of theory and experiment in the determination of the adsorption sites and configurations warrants the extension of the DFT analysis to reaction barriers and binding energies of the molecules and reaction intermediates involved in the selective hydrogenation, $C_2H_2 + H_2 \rightarrow C_2H_4$. To reveal trends in activity and selectivity for the different structures of Pd₃ and Pd₁, we compare the reaction barrier heights as summarized in Figure 7. The energy step diagram is to be read from left to

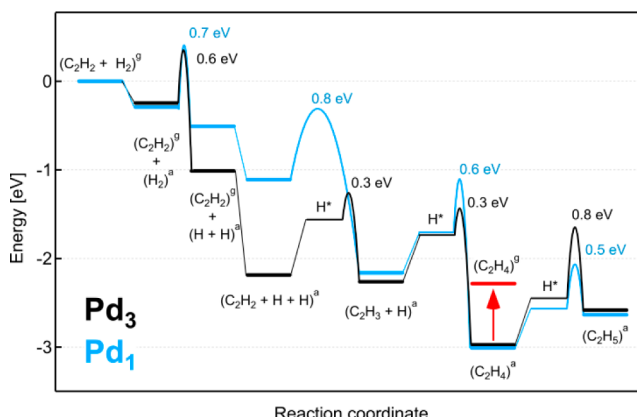


Figure 7. DFT computed energies of the intermediate states (horizontal lines) and barrier heights (inverted parabolas) for the semihydrogenation of acetylene on the two surface terminations Pd₃ and Pd₁. Metastable hydrogen diffusion steps (see main text for details) are indicated by “H*”. The superscript “g” and “a” signals the gaseous and adsorbed state of a molecule, respectively. Figure 2 shows the respective bonding geometries, and numerical values of energy differences are given in the text.

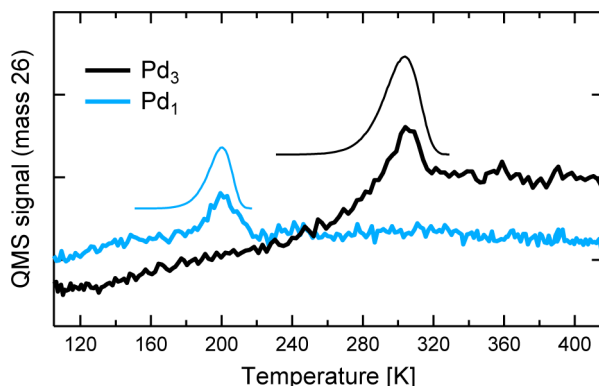


Figure 6. C₂H₂ desorption (mass 26) during a TPD ramp (6 K/s) for Pd₃ and Pd₁, after exposure to 0.1 Langmuir at 77 K. The fitted peaks (thin lines above the experimental data) correspond to binding energies of -0.52 and -0.80 eV for Pd₁ and Pd₃, respectively, and were obtained from the Redhead equation.²³

right, with the total energies relative to the initial condition of C₂H₂ and H₂ in the gaseous state. For the exact geometric reaction pathway the reader is referred to the SI.

For the cases of surfaces with separated active sites as investigated here, the reactants bind at much larger distances from each other than on single element metal surfaces. Thus, the approach of the reactants to a nearby metastable position (marked H* in Figure 7) has to be considered explicitly, and the respective energetic cost has to be taken into account. In

our analysis, we split the hydrogenation reactions into two parts: The first step involves the hydrogen transport from the most favorable adsorption site to a metastable adsorption position close to the hydrocarbon (H^*). The second step represents the actual hydrogenation reaction barrier, which was calculated (inverted parabolas in Figure 7) using NEB starting from the hydrogen in the metastable position (see SI for details).

The first step considered in the DFT approach is the adsorption and dissociation of H_2 , yielding comparable energies and barriers, which might be rate limiting for the overall reaction on the two surfaces. For atomic hydrogen the most preferred site is a hollow site on a Pd trimer,¹¹ as shown in Figure 2. On Pd_1 , this site belongs to the third atomic layer which is strongly coordinated by the substrate atoms, resulting in a lower hydrogen adsorption energy as compared to Pd_3 . Given the very small distance between the layers of 143 pm, the H atom is still available for hydrogenation reactions. For the first hydrogenation step, namely the transformation of acetylene into C_2H_3 (vinyl), we consider the two acetylene configurations shown in Figure 2.

On the Pd_3 surface, the hydrogen approach (to H^*) is endothermic by 0.7 eV. The subsequent hydrogenation process requires overcoming a barrier of 0.3 eV, which results in a total reaction barrier of 1.0 eV.

On the Pd_1 surface, where two degenerate C_2H_2 adsorption positions exist (compare Figure 2B), the barrier for hydrogenation of acetylene bound in the $\pi/di-\sigma$ conformation, i.e., partially bound to subsurface Ga, is lower (barrier height: 0.8 eV) than for hydrogenation from the π -bonded, i.e., on-top Pd position (barrier height 1.1 eV). For simplicity, only the first case is drawn in the energy step diagram in Figure 7. The main reason for the lower barrier from the $\pi/di-\sigma$ conformation is that hydrogen is supplied directly from its energetically most favored position, such that no endothermic hydrogen diffusion to a metastable position is required.

For C_2H_3 on Pd_3 , the most favored adsorption conformation exhibits a tilted C–C bond with respect to the surface plane, with the lower C atom close to the center of the Pd hollow site. Similar geometries were found by theory and experiment for Pd(111).^{19,24} The conformation is very different on Pd_1 , where the C–H group relaxes to a bridge site position between the topmost Pd and a subsurface Ga atom, while the C–H₂ group is tilted toward the topmost Pd atom. This situation is similar to that reported for C_2H_3 on PdGa(210).²²

The next step of the reaction is hydrogenation of vinyl toward ethylene. This reaction requires overcoming barriers of 0.8 and 1.1 eV for Pd_3 and Pd_1 , respectively, including the hydrogen diffusion to the metastable position (H^* , endothermic by 0.5 eV for both surfaces).

As presented within the discussion on the LT-STM results, ethylene adsorbs in π -bonded conformations on top of Pd atoms of the terminating layer for both surfaces and the binding energies amount to -0.73 eV on Pd_1 and -0.69 eV on Pd_3 (see red line in Figure 7). Once formed, the question arises whether ethylene would leave the surface (beneficially affecting selectivity) or remain and undergo further hydrogenation (compromising selectivity). The crucial parameter for this step is the barrier height for further hydrogenation.

For the transformation to ethyl (C_2H_5) on Pd_1 we find an endothermic process (by 0.38 eV). The endothermic hydrogen diffusion to the metastable site (H^* , 0.4 eV) and the subsequent hydrogenation reaction barrier (0.5 eV) result in

a total barrier of 0.9 eV. This value is only marginally higher than the desorption energy of ethylene (0.73 eV) on this surface; hence we cannot exclude the further transformation to ethyl. On Pd_3 , on the contrary, the barrier for further hydrogenation of ethylene is instead 1.3 eV (including 0.8 eV for the hydrogen approach). This is almost double compared to the ethylene binding energy (-0.69 eV), making desorption much more likely.

To compare the two three-fold PdGa surfaces with respect to their efficiency as catalysts, the energy step diagram shown in Figure 7 should be interpreted with regard to the following criteria: (a) acetylene and hydrogen (the reactants) have a sufficiently high binding energy to allow hydrogenation on the surface; (b) hydrogen dissociation is thermodynamically favorable on the surface; (c) the hydrogenation process of acetylene has a high yield resulting from low-reaction barriers; and (d) there exist mechanisms hindering a further hydrogenation of ethylene and avoiding the formation of heavier hydrocarbons.

In almost all of the criteria named above, the Pd_3 is superior to the Pd_1 termination; adsorption energy of acetylene is larger (a), hydrogen dissociation is more exothermic (b), and the barrier toward (over-) hydrogenation to C_2H_5 is higher (d). Furthermore, if a situation of excess hydrogen is considered, all favored hydrogen adsorption sites and the metastable sites can be considered to be dynamically occupied on both surfaces. As a consequence, the hydrogenation will mostly start from the metastable positions, closer to the hydrocarbon. This leads to a considerable decrease of the barrier heights (and thus increase in activity) for the hydrogenation steps (c) which is much more pronounced on Pd_3 as compared to Pd_1 (cf. Figure 7). Additionally, on Pd_1 , the binding energy for ethylene (-0.73 eV) is found larger than for acetylene (-0.61 eV). As a consequence, the catalytic surface would become inactive due to ethylene poisoning, in particular when used in ethylene rich streams as purification catalyst.

Our DFT results are in general agreement with the very recently published investigation of the semihydrogenation on PdGa surfaces by Krajci and Hafner.²⁵ Furthermore, our DFT results compare to those found for the same reaction on the (210) surface of the PdGa compound.²² However, two differences should be pointed out: First, the binding energy of atomic hydrogen is much stronger for the three-fold surfaces (Pd_3 : $E_{b,H} = -0.51$ eV, Pd_1 : -0.25 eV, PdGa(210): $E_{b,H} = -0.06$ eV), which is assigned to the Pd hollow sites that are present on Pd_3 and Pd_1 . And second, the barriers toward further hydrogenation to C_2H_5 are lower on the (210) surface as compared to Pd_3 (Pd_3 : 0.8 eV, Pd_1 : 0.5 eV, PdGa(210): 0.5 eV). In comparison to DFT simulations of the reaction on the close-packed Pd(111) surface by Sheth et al.,¹⁹ the intermetallic Pd_3 surface yields lower reaction barriers for the considered hydrogenations toward ethylene and should thus yield higher activity (Pd(111): 0.68, 0.88, and 0.72 eV for the step toward C_2H_3 , C_2H_4 and C_2H_5 , respectively). However, quantitative comparison to the different *ab initio* results has to be done with care, as the different computational parameters and the choice of exchange functionals may alter the results.

5. CONCLUSIONS

We compared the PdGa:A(111) and (-1-1-1) model catalyst surfaces exhibiting separated single Pd atoms (Pd_1) and Pd trimers (Pd_3) respectively, with regard to the adsorption of small hydrocarbons. In the combined STM and DFT study, we

found that the single (Pd_1) and three-atomic (Pd_3) Pd ensembles which provide the lowest energy adsorption sites for CO^{12} also play the major role in the bonding of H_2 , C_2H_2 , and C_2H_4 . However, for the single atomic Pd sites of Pd_1 , the Ga atoms of the second layer are involved in C_2H_3 bonding and in the second favorite adsorption site for C_2H_2 . DFT and TPD reveal a weaker π -bond of acetylene to the single atomic Pd sites, as compared to the $\pi/di-\sigma$ bonding to the Pd trimers on Pd_3 . Also the binding energy of atomic hydrogen is significantly higher on Pd_3 than on Pd_1 , while it is similar for molecular hydrogen and ethylene.

Based on the agreement of experiment and quantum chemical calculations of the adsorption, we expanded the DFT study to compute the reaction step energies and barrier heights for the semihydrogenation reaction pathway of acetylene toward the desired product ethylene. We found that the hydrogen approach toward the hydrocarbon plays a crucial role in the energetics of the reaction, leading to reduced reaction barriers for one of the three-fold PdGa surfaces (namely Pd_3) in the case of hydrogen excess. This is attributed to the terminating Pd layer, consisting of atomic trimers, which allow for binding of both reactants simultaneously in a metastable configuration. If the hydrogen is supplied from the energetically most favored H adsorption site, the barrier heights for the reaction steps were found similar on the two surfaces, except for the step toward ethyl (C_2H_5), where the barrier on Pd_3 is larger compared to that for Pd_1 , enhancing selectivity.

The comparison of three and single Pd atom catalytic ensembles presented here reveals that the surface structure on the smallest possible length scale has a strong influence on the binding properties and on the catalytic reaction pathways. This opens the possibility to design improved catalysts by the choice of idealized surface atomic structures. As in the case of the PdGa surfaces, an experimental confirmation of the computed selectivity and activity differences would corroborate this approach.

ASSOCIATED CONTENT

Supporting Information

STM images on tip-induced diffusion and reorientation of adsorbed molecules as well as details on the DFT method and the computed reaction pathways are given. This material is available free of charge via the Internet at <http://pubs.acs.org>.

Web-Enhanced Feature

An STM video of 30 s (taken over a period of 4 h), resolving the molecular rotation of single C_2H_2 molecules on the Pd_3 trimers is available in the HTML version of the paper.

AUTHOR INFORMATION

Corresponding Authors

Daniele.Passerone@empa.ch

Jan.Prinz@empa.ch

Notes

The authors declare no competing financial interest.

ACKNOWLEDGMENTS

We gratefully acknowledge funding by the Swiss National Science Foundation under the contract 200021-129511 and support by the Swiss National Supercomputing Center (CSCS). We thank Karl Heinz Ernst and the members of the COST Action CM0904 for fruitful discussions.

REFERENCES

- (1) Molnar, A.; Sarkany, A.; Varga, M. *J. Mol. Catal. A: Chem.* **2001**, 173, 185.
- (2) Borodzinski, A.; Bond, G. C. *Catal. Rev.: Sci. Eng.* **2008**, 50, 379.
- (3) Armbrüster, M.; Kovnir, K.; Behrens, M.; Teschner, D.; Grin, Y.; Schlägl, R. *J. Am. Chem. Soc.* **2010**, 132, 14745.
- (4) Sachtle, W. M. H. *Catal. Rev.: Sci. Eng.* **1976**, 14, 193.
- (5) Allison, E. G.; Bond, G. C. *Catal. Rev.: Sci. Eng.* **1972**, 7, 233.
- (6) Kovnir, K.; Armbrüster, M.; Teschner, D.; Venkov, T. V.; Jentoft, F. C.; Knop-Gericke, A.; Grin, Y.; Schlägl, R. *Sci. Technol. Adv. Mater.* **2007**, 8, 420.
- (7) Piccolo, L. *Chem. Commun.* **2013**, 49, 9149.
- (8) Armbrüster, M.; Kovnir, K.; Friedrich, M.; Teschner, D.; Wowsnick, G.; Hahne, M.; Gille, P.; Szentmiklosi, L.; Feuerbacher, M.; Heggen, M.; Girgsdies, F.; Rosenthal, D.; Schlogl, R.; Grin, Y. *Nat. Mater.* **2012**, 11, 690.
- (9) Kovnir, K.; Armbrüster, M.; Teschner, D.; Venkov, T. V.; Szentmiklosi, L.; Jentoft, F. C.; Knop-Gericke, A.; Grin, Y.; Schlägl, R. *Surf. Sci.* **2009**, 603, 1784.
- (10) Armbrüster, M.; Borrman, H.; Wedel, M.; Prots, Y.; Giedigkeit, R.; Gille, P. Z. *Kristallogr. - New Cryst. Struct.* **2010**, 225, 617.
- (11) Prinz, J.; Gaspari, R.; Pignedoli, C. A.; Vogt, J.; Gille, P.; Armbrüster, M.; Brune, H.; Gröning, O.; Passerone, D.; Widmer, R. *Angew. Chem., Int. Ed.* **2012**, 51, 9339.
- (12) Prinz, J.; Gaspari, R.; Stoeckl, Q. S.; Gille, P.; Armbrüster, M.; Brune, H.; Gröning, O.; Pignedoli, C. A.; Passerone, D.; Widmer, R. *J. Phys. Chem. C* **2014**, 118, 12260–12265.
- (13) Gille, P.; Ziener, T.; Schmidt, M.; Kovnir, K.; Burkhardt, U.; Armbrüster, M. *Intermetallics* **2010**, 18, 1663.
- (14) VandeVondele, J.; Krack, M.; Mohamed, F.; Parrinello, M.; Chassaing, T.; Hutter, J. *Comput. Phys. Commun.* **2005**, 167, 103.
- (15) Perdew, J. P.; Burke, K.; Ernzerhof, M. *Phys. Rev. Lett.* **1997**, 78, 1396.
- (16) Henkelman, G.; Überuaga, B. P.; Jonsson, H. *J. Chem. Phys.* **2000**, 113, 9901.
- (17) Dunphy, J. C.; Rose, M.; Behler, S.; Ogletree, D. F.; Salmeron, M.; Sautet, P. *Phys. Rev. B: Condens. Matter Mater. Phys.* **1998**, 57, 12705.
- (18) Ibach, H.; Lehwald, S. *J. Vac. Sci. Technol.* **1978**, 15, 407.
- (19) Sheth, P. A.; Neurock, M.; Smith, C. M. *J. Phys. Chem. B* **2003**, 107, 2009.
- (20) Sesselmann, W.; Woratschek, B.; Ertl, G.; Kuppers, J.; Haberland, H. *Surf. Sci.* **1983**, 130, 245.
- (21) Neurock, M.; van Santen, R. A. *J. Phys. Chem. B* **2000**, 104, 11127.
- (22) Krajci, M.; Hafner, J. *J. Catal.* **2012**, 295, 70.
- (23) Redhead, P. A. *Vacuum* **1962**, 12, 274.
- (24) Stacchiola, D.; Calaza, F.; Zheng, T.; Tysoe, W. T. *J. Mol. Catal. A: Chem.* **2005**, 228, 35.
- (25) Krajci, M.; Hafner, J. *J. Catal.* **2014**, 312, 232.

Supporting Information

"Adsorption of Small Hydrocarbons on the threefold PdGa surfaces: The Road to Selective Hydrogenation"

Jan Prinz*, Carlo A. Pignedoli, Quirin S. Stöckl,† Marc Armbrüster,‡ Harald Brune,‡ Oliver Gröning, Roland Widmer and Daniele Passerone*

Empa. Swiss Federal Laboratories for Materials Science and Technology, nanotech@surfaces Laboratory, Ueberlandstrasse 129, 8600 Dübendorf, Switzerland.

† Empa. Swiss Federal Laboratories for Materials Science and Technology, Nanoscale Materials Science, Ueberlandstrasse 129, 8600 Dübendorf, Switzerland.

* Max-Planck-Institut für Chemische Physik fester Stoffe, 01187 Dresden, Germany

‡ Institute of Condensed Matter Physics, Station 3, Ecole Polytechnique Fédérale de Lausanne (EPFL), 1015 Lausanne, Switzerland.

In the following supporting information we will define the PdGa:A(-1-1-1)Pd₃ terminated by three Pd atoms as Pd₃ and the PdGa:A(111)Pd₁ terminated by one Pd atom as Pd₁.

S1. STM of small molecular adsorbates on the PdGa(111) surfaces

Tip induced hopping of H₂

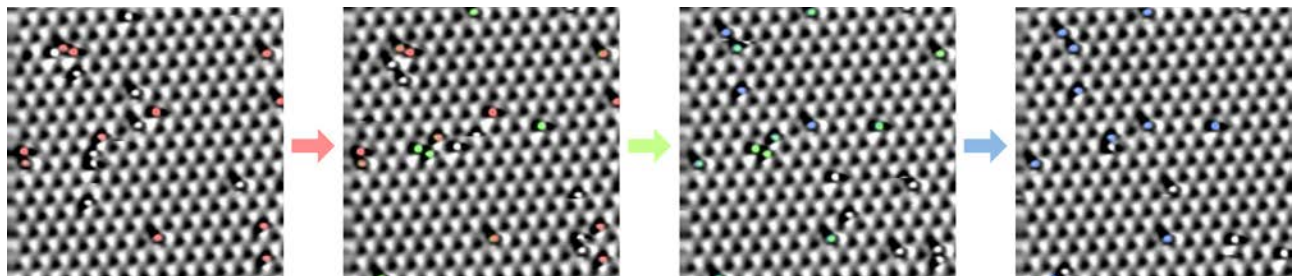


Figure S1: Tip induced hopping of H₂ molecules on the Pd₃ surfaces at 5K. Images were taken in upwards scan with a period of 1 minute. As a guide to the eye, those molecules that maintain their position in two subsequent images are color coded. (10 x 10 nm, tunnel parameters: -5 mV, 1nA)

Collective alignment of neighboring C₂H₂ on Pd₃

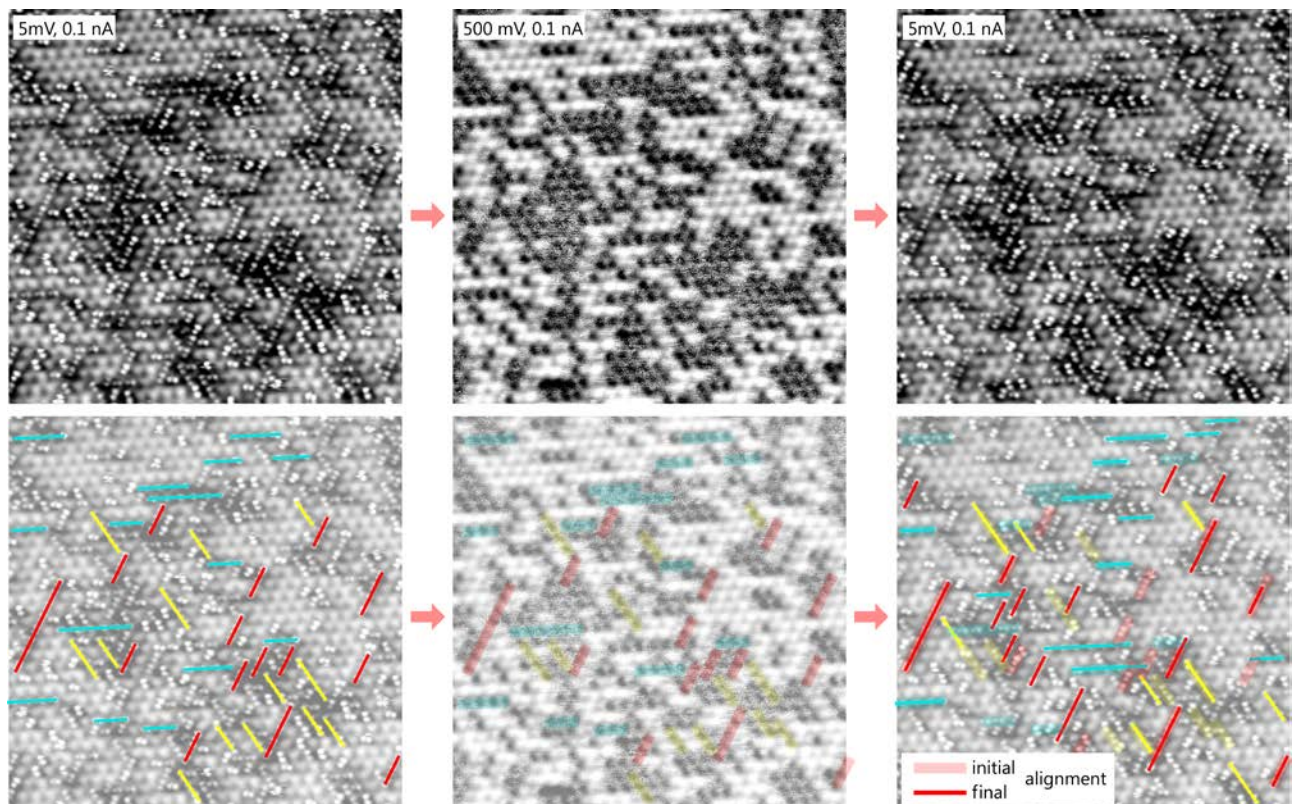


Figure S2: Top: Three subsequent STM images (20 x 20 nm) of C₂H₂ molecules on PdGa:A:(-1-1-1)Pd₃ at 5 K. Middle: Increasing the tunnel voltage from 5 mV to 500 mV leads to a re-arrangement of the collective orientations. Bottom: alignments of three or more adsorbates are marked with colored lines, color coded for the three symmetry-equivalent directions.

Tip induced change of adsorption site of C₂H₂ on Pd₁

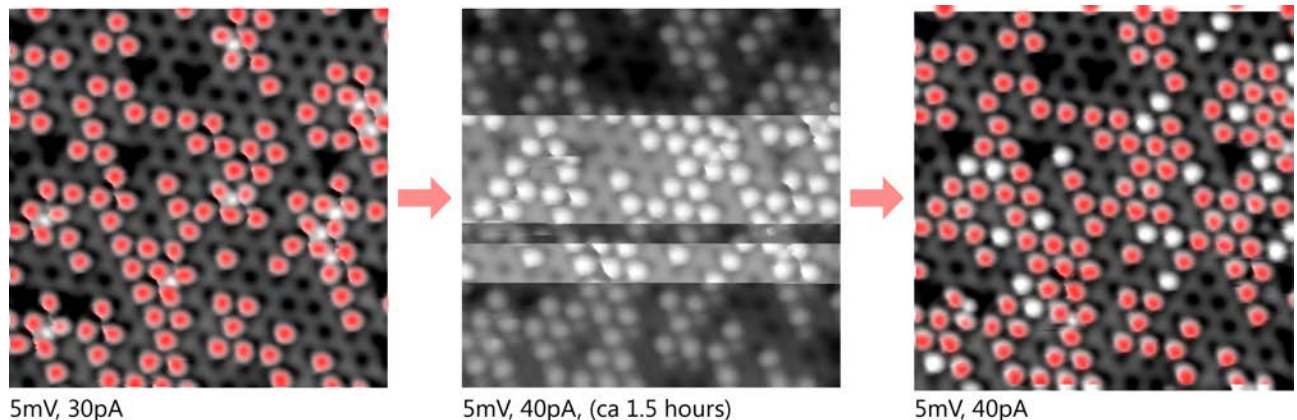


Figure S3: Tip induced relaxation of C₂H₂ adsorbed in the interstitial adsorption site on Pd₁. A slight increase in tunneling current (30 pA → 40 pA) first leads to unstable imaging conditions and tip changes (center). After scanning the same area for about 1.5 hours, conditions have stabilized and almost all interstitial adsorbates have disappeared. Instead the number of on-top adsorbed C₂H₂ has increased. Protrusions that were present initially are marked in red.

Steric repulsion of neighboring C₂H₄ molecules on Pd₃

For neighboring C₂H₄ molecules on Pd₃, a slight shift is observed with respect to the position found for a single molecule on the Pd trimer. The STM images in overlay with the DFT structures are shown below.

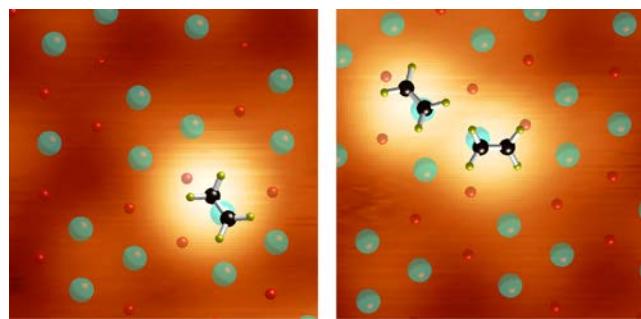


Figure S4: Steric repulsion of neighboring C₂H₄ molecules adsorbed on the same Pd trimer on PdGa:A(-1-1-1)Pd₃. The adsorption energy per molecule accounts to 0.69 eV and 0.50 eV for the left and right case, respectively.

S2. Details on the computational methods

Details on the computational methods

All calculations were performed in the mixed Gaussian plane wave approach as implemented in the CP2K code (<http://www.cp2k.org>). The substrate was modeled in the repeated slab geometry. Test performed on slabs thicker than 23/24 atomic layers confirm that the thickness of our slab is appropriate. Norm conserving pseudopotentials of the Goedecker type were employed.¹ Semicore 4s and 4p states of Pd, as well as 3d semicore states of Ga, were treated in the valence. A cutoff of 600 Ry was used for the representation of the charge density in plane waves. We used the PBE parameterization for the exchange correlation functional.²

The Nudged Elastic Band method

NEB calculations were performed in the “Climbing Image” scheme.³ Every reaction path was split in order to contain a single transition state per NEB simulation. According to the complexity of the NEB simulation we employed 10 to 31 images in the path. To increase precision for the determination of the total energies separate DFT relaxations were performed for the metastable positions of hydrogen.

Particular care was dedicated to the creation of the initial guess for each NEB simulation: starting from a given equilibrium geometry a series of consecutive constrained optimizations, where the distance between a H atom and a C atom in an adsorbed molecule was varying, allowed to select snapshots of a minimally biased reaction sequence. NEB procedure was then iterated until convergence of the barrier to 0.1 eV was reached.

S3. Details on DFT computed hydrocarbon adsorption geometries

C₂H₂ adsorption on Pd₃

In this case, the adsorbate is bound in a π /di- σ bond-configuration to the Pd trimer, with an energy of 1.17 eV. The C-C-H bonds are slightly asymmetrically tilted with 49.5° and 51.5°, resulting in a different height of the H atoms above the surface plane. Also for this surface we tested a π /di- σ configuration to Ga (similar to the one found for Pd₁), shown in the inset below, yielding an unfavorable adsorption energy of 0.3 eV.

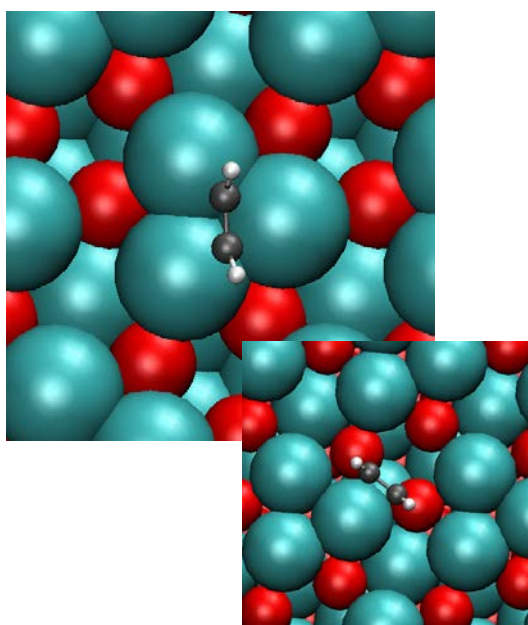


Figure S5: Top: Favored adsorption configuration for C₂H₂ on Pd₃, which is very similar to the one found on Pd(111). The inset shows the adsorption on the Ga atoms of the 2nd layer, similar to that found for Pd₁ (see Figure S6). However, on Pd₃ this configuration yields an adsorption energy of only 0.3 eV, and is thus unfavorable.

C₂H₂ adsorption on Pd₁

Acetylene binds on this surface with an on-top geometry where the C-C-H bond angle is rotated by 18° with respect to the linear configuration. The adsorption energy amounts to 0.61 eV. The adsorption energy for other tested configurations shown in the bottom left) amounts to 0.43 eV, whereas it is 0.60 eV for the di sigma configuration shown in the bottom right. Given the almost perfect degeneracy of the on-top site and the di-sigma configuration to Ga, we will consider paths leading from both configurations to the C₂H₃ geometry (see below).

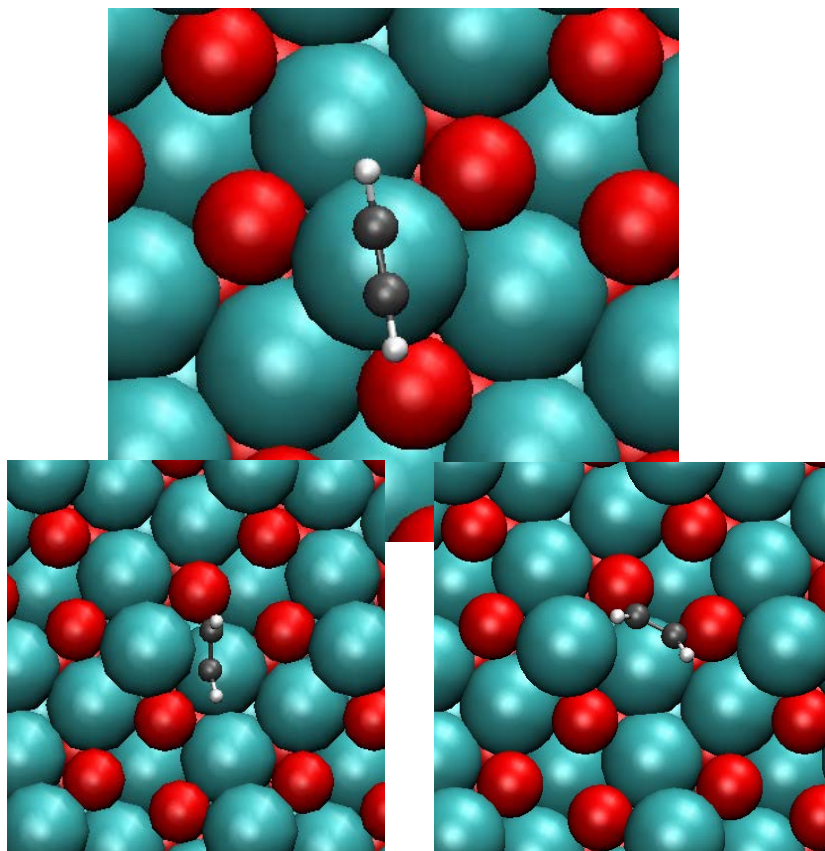


Figure S6: Three different adsorption configurations for C₂H₂ on Pd₁ yielding adsorption energies of 0.61 eV, 0.43 eV and 0.60 eV for the situations shown in the top, bottom left, and bottom right panel, respectively.

C₂H₃ adsorption on Pd₃

The adsorption occurs on the trimer, and the configuration has a gain in energy of 0.076 eV with respect to C₂H₂ adsorption.

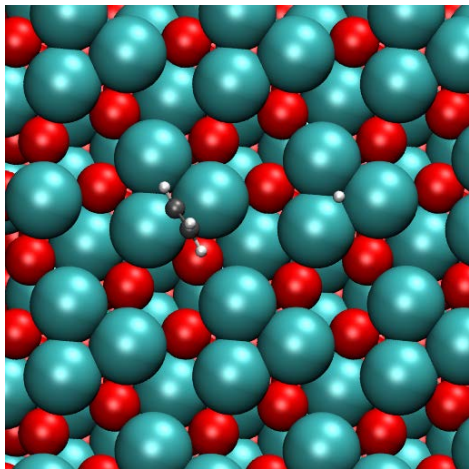


Figure S7: The favored adsorption site after the first hydrogenation step is a bridge site between two Pd atoms of the trimer, yielding only a small energy gain of 0.076 eV with respect to C₂H₂. The C-C axis of the C₂H₃ molecule is tilted with respect to the surface plane.

C₂H₃ adsorption on Pd₁

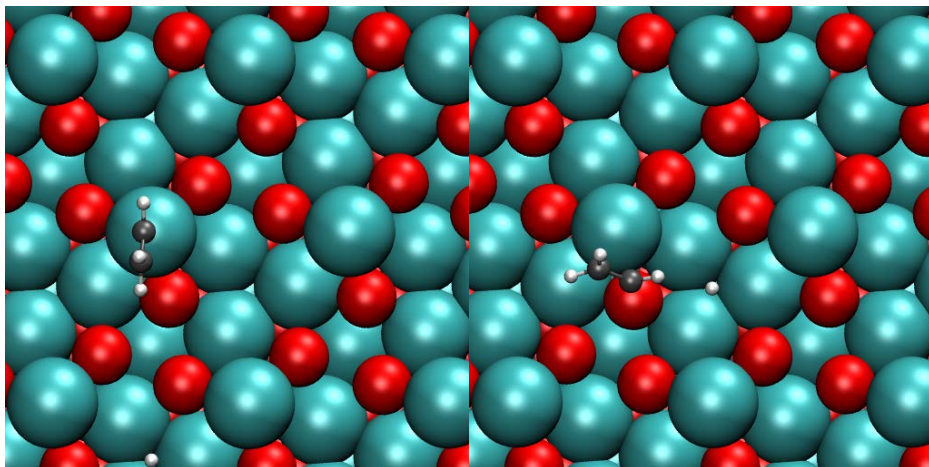


Figure S8: The configuration shown in the right panel is more stable by 0.66 eV compared to the on-top Pd position shown in the left panel. As for C₂H₂, adsorption (see Figure S6), an adsorption site involving 2nd layer Ga atoms is identified for this surface.

S4. Details on NEB computed reaction barriers

$\text{H}_2 \rightarrow \text{H} + \text{H}$ on Pd_3

In all panels of this kind the geometries at selected points of the trajectory (yellow symbols) will be shown on the left hand side, together with the reaction barrier below. In the right panel, the path of hydrogen and hydrocarbons from the initial (white) to the final (black) state is presented.

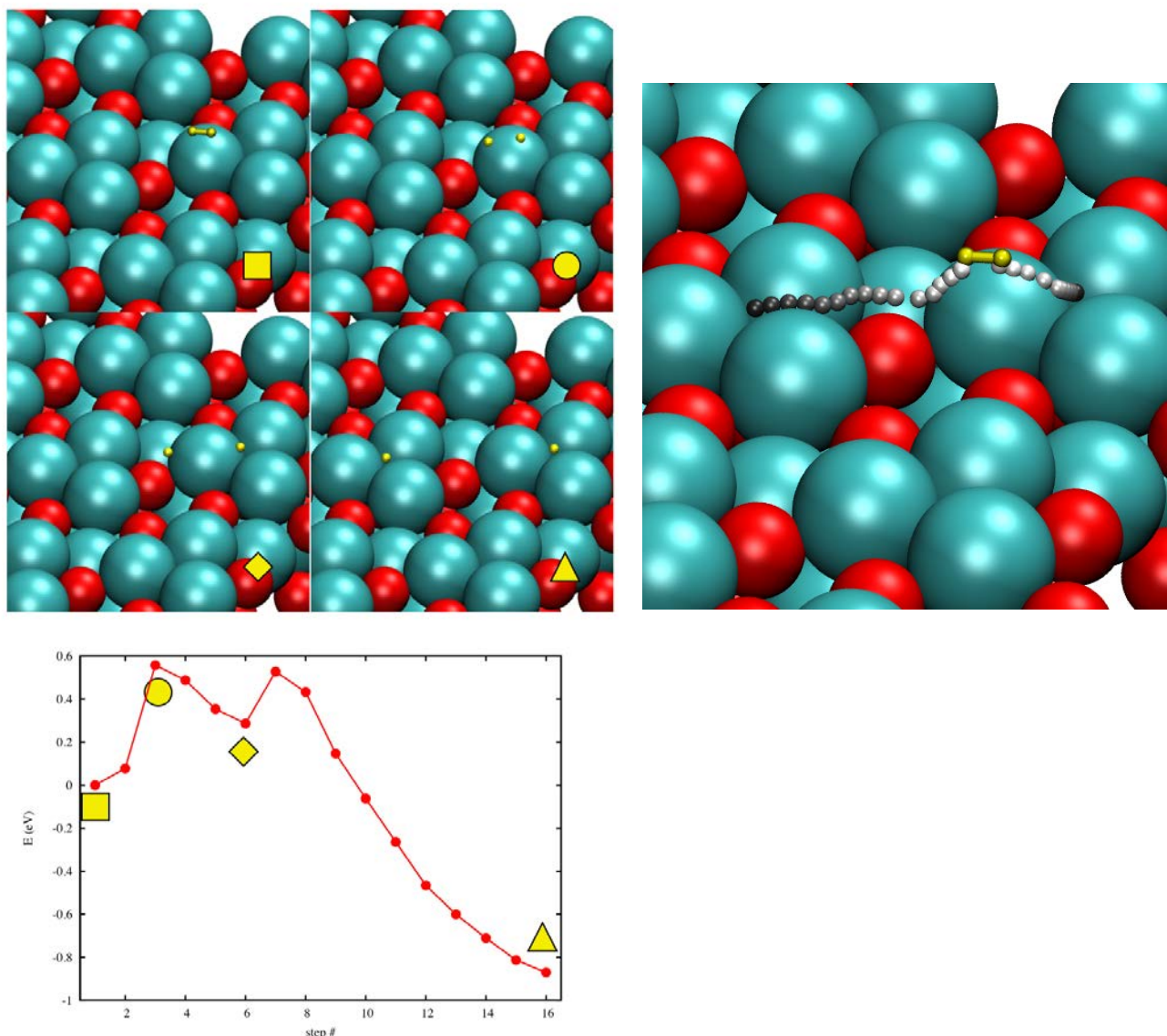


Figure S9: Hydrogen dissociation requires overcoming a barrier of 0.55 eV. The first minimum is due to one H atom in a metastable position.

$\text{H}_2 \rightarrow \text{H} + \text{H}$ on Pd_1

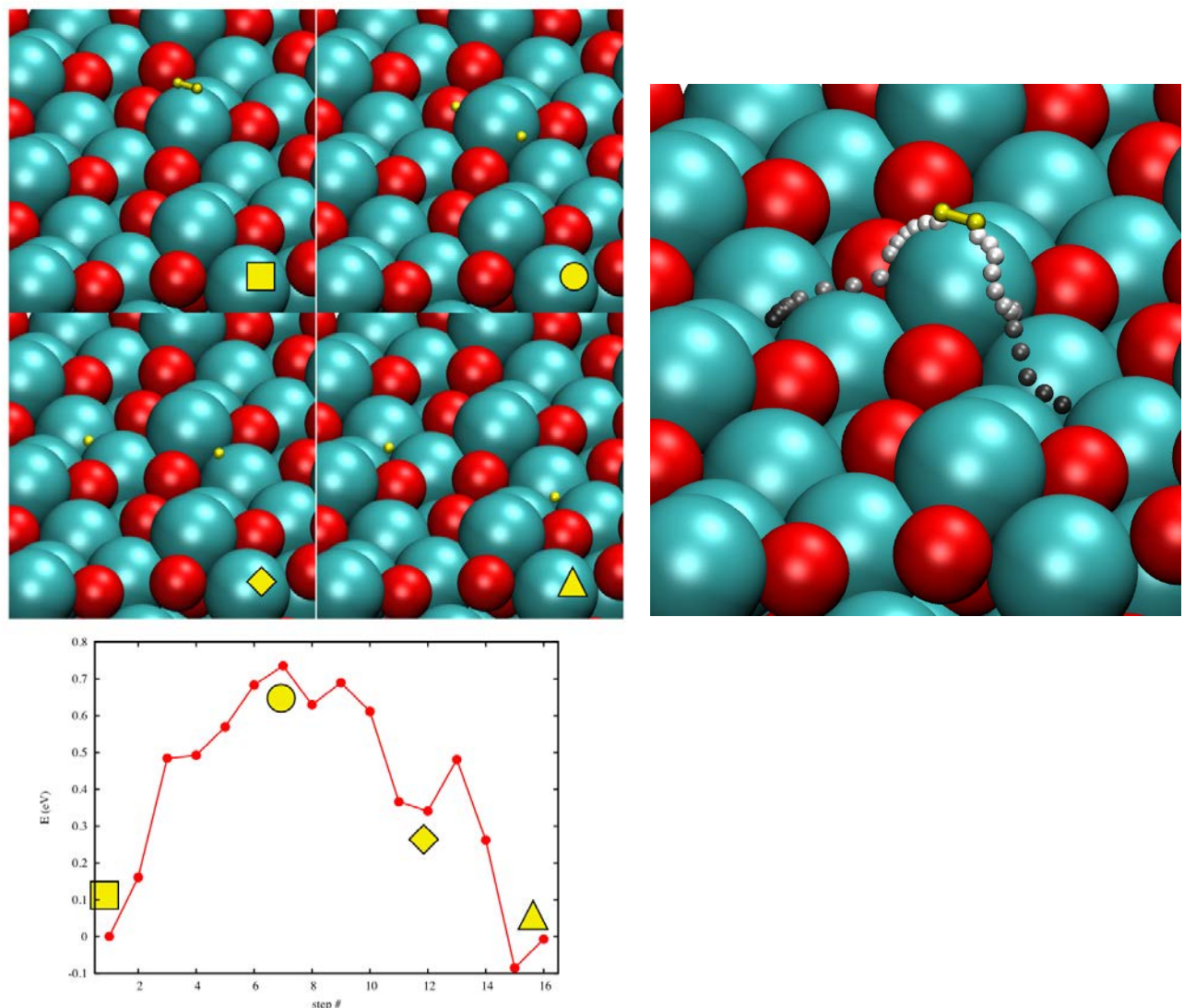


Figure S10: The barrier for hydrogen dissociation on Pd_1 is computed to 0.72 eV, with only a small gain in total energy.

$\text{C}_2\text{H}_2 \rightarrow \text{C}_2\text{H}_3$ on Pd_3

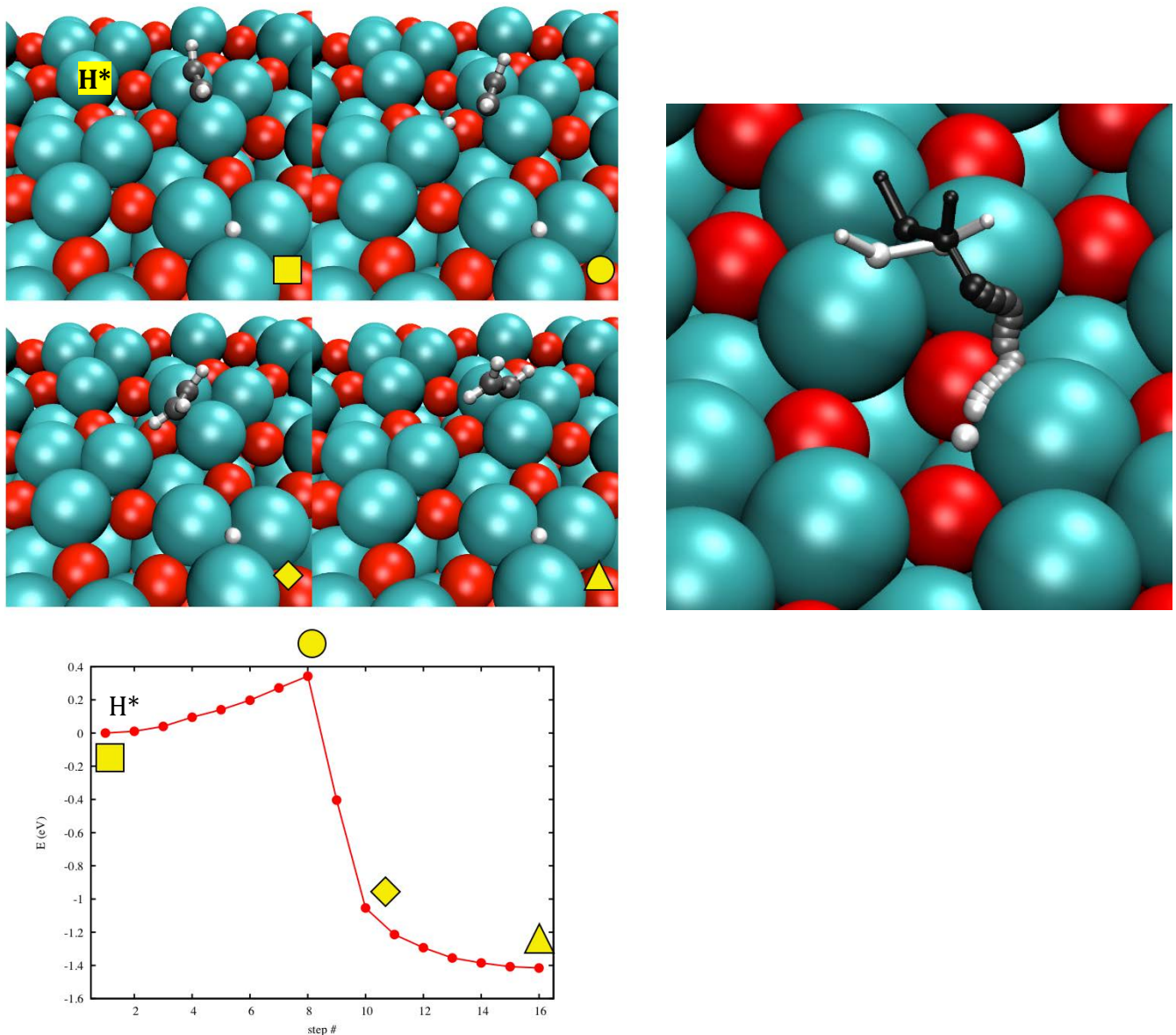


Figure S11: The first hydrogenation step on Pd_3 requires a precedent endothermic (0.7 eV) approach of the atomic hydrogen towards the hydrocarbon (not shown in the graph) into a metastable position H^* . The hydrogenation barrier from the metastable hydrogen position is very low with 0.34 eV.

$\text{C}_2\text{H}_2 \rightarrow \text{C}_2\text{H}_3$ on Pd_1

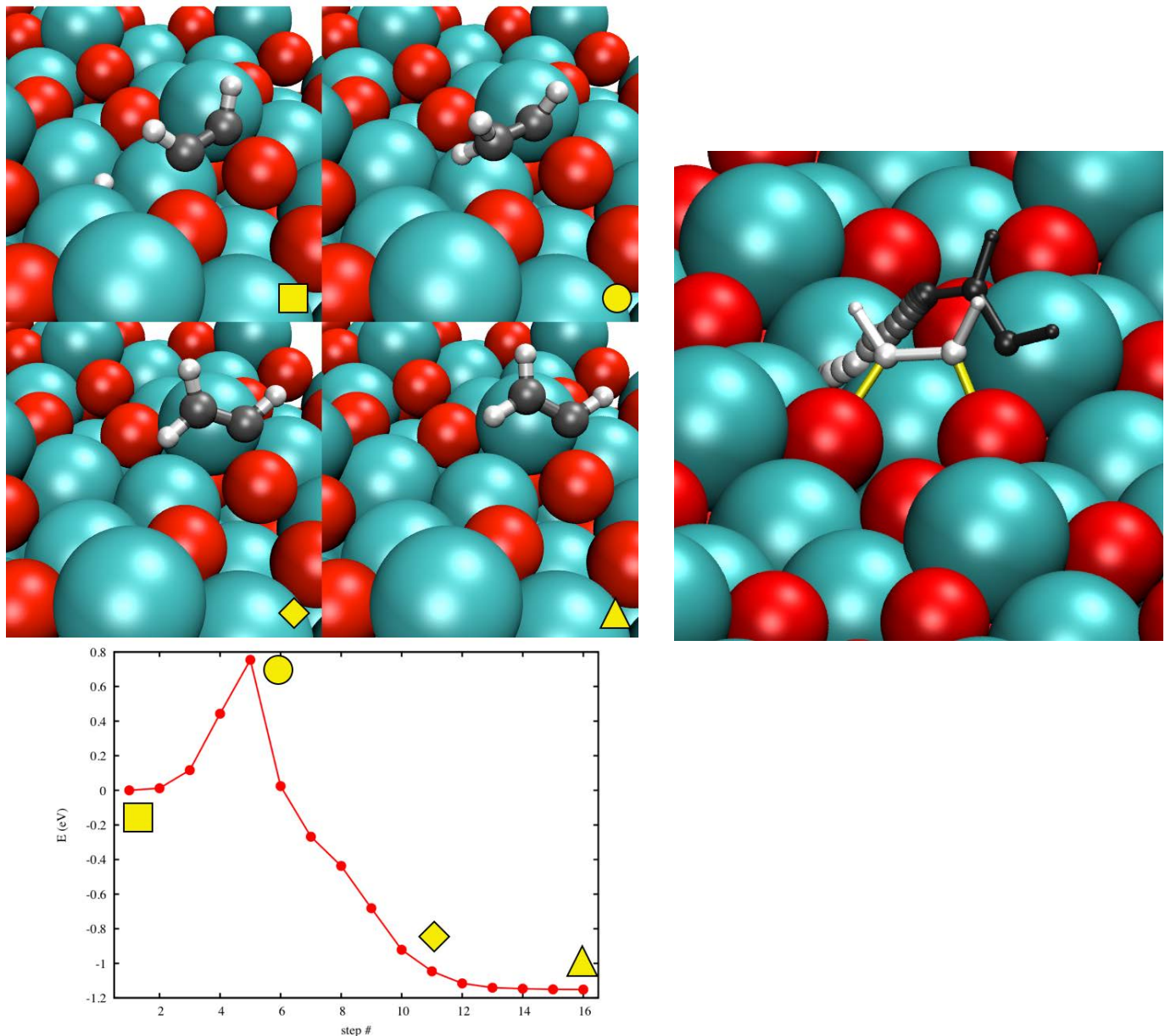


Figure S12: The first NEB simulated reaction connects the alternative $\pi/\text{di-}\sigma$ Ga configuration for acetylene (Figure S6, bottom right panel) to the favorable adsorption geometry for C_2H_3 (Figure S8, right panel). As the hydrogen is supplied from the hollow site of the 3rd layer Pd trimer, no additional barrier is present for the hydrogen approach.

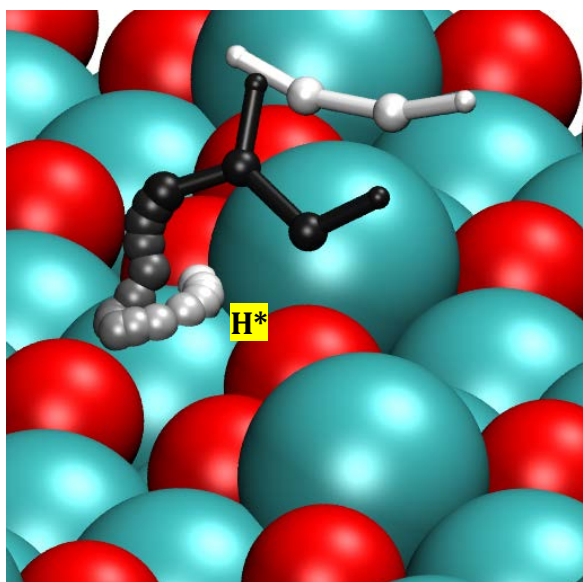


Figure S13: The second NEB path is connecting the on-top π configuration for C_2H_2 (Figure S6, top panel) with the bridge site energetic minimum of C_2H_3 (Figure S8, right panel). (This reaction barrier is not shown in Figure 7 of the main text.) The hydrogenation barrier amounts to 0.62 eV. The precedent hydrogen approach step (not shown) would cost additional 0.6 eV, which makes this reaction path less likely than the one starting from C_2H_2 in a $\pi/\text{di-}\sigma$ Ga bridge state, shown in Figure S12.

$\text{C}_2\text{H}_3 \rightarrow \text{C}_2\text{H}_4$ on Pd_3

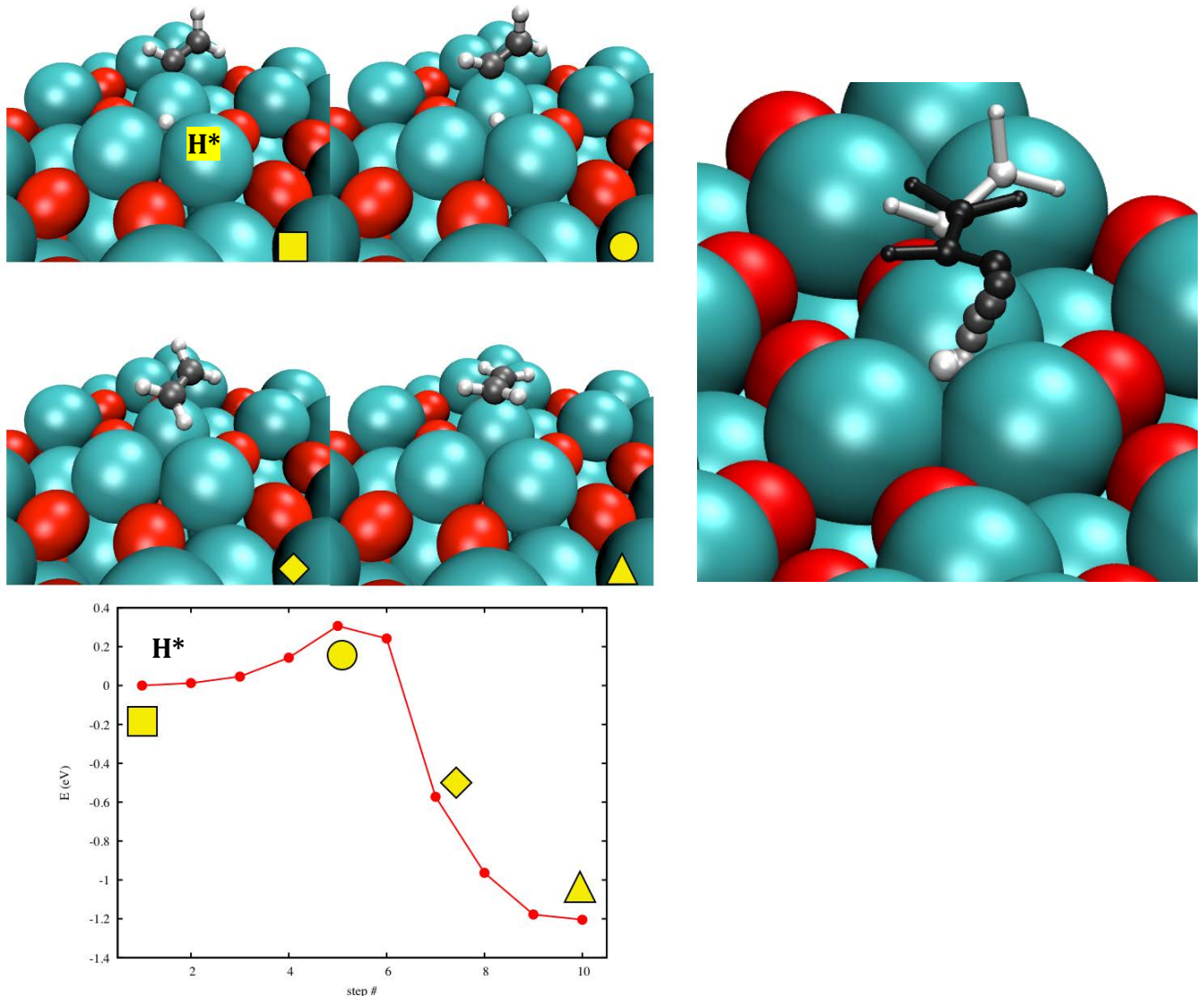


Figure S14: To achieve hydrogenation, the hydrogen has to diffuse in an endothermic step (H^* , 0.5 eV) to the trimer hosting the vinyl (■). The co-adsorption on the same trimers leads to a shift of the vinyl from the preferred bridge site (Figure S7) to an on-top site position on Pd . The NEB presented above starts from this situation, yielding a reaction barrier of 0.3 eV for the hydrogenation step(●).

$\text{C}_2\text{H}_3 \rightarrow \text{C}_2\text{H}_4$ on Pd_1

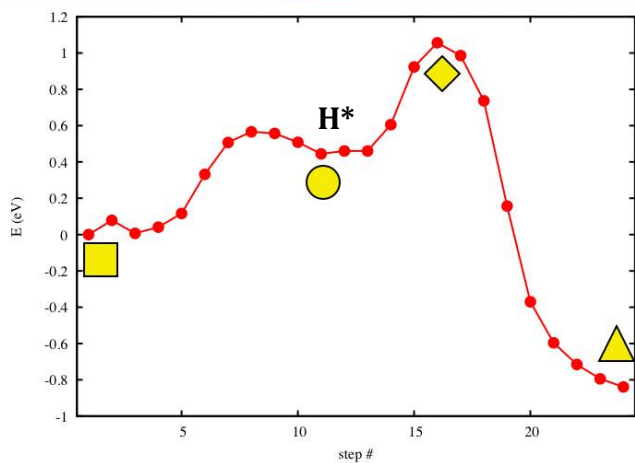
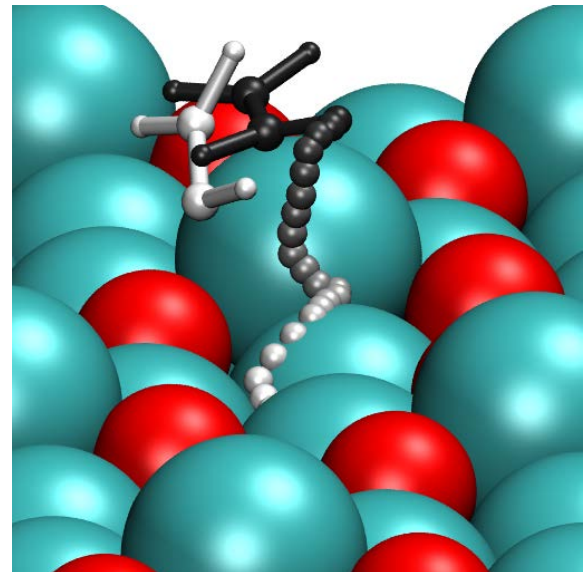
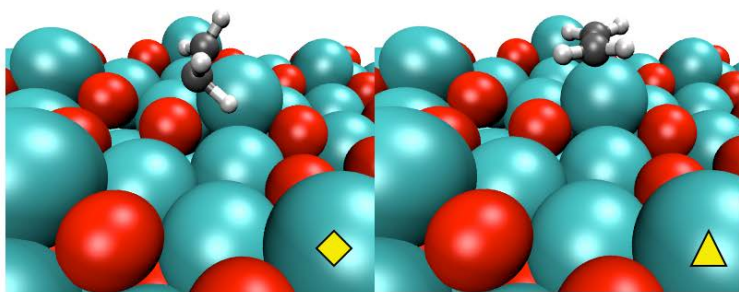
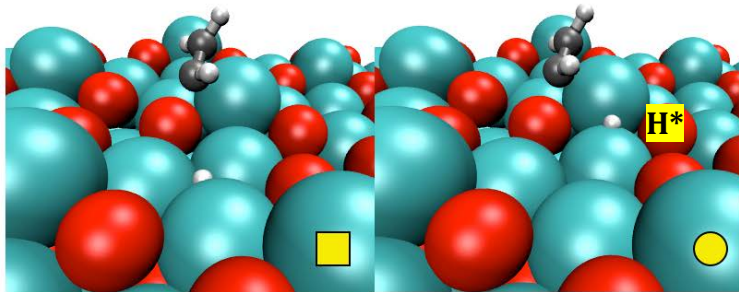


Figure S15: In the case of Pd_1 , we split the NEB in two different calculations to test the diffusion of atomic hydrogen. To reach the metastable position (\bullet), an initial barrier of 0.6 eV has to be overcome. The following the attack of the vinyl fragment yields a further barrier of 0.6 eV leading to the more stable ethylene state on-top of the outermost Pd atom (\blacktriangle).

$\text{C}_2\text{H}_4 \rightarrow \text{C}_2\text{H}_5$ on Pd_3

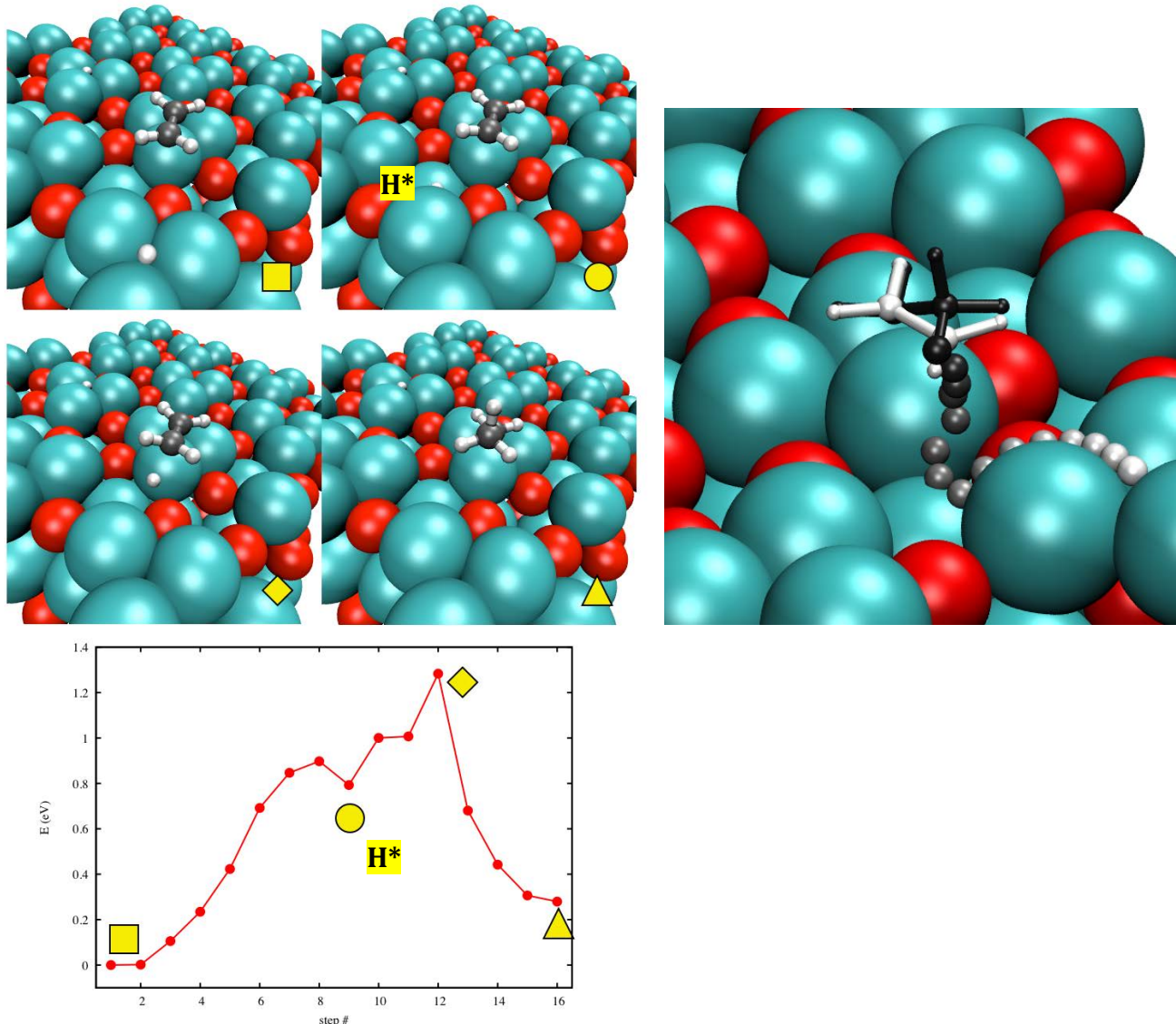


Figure S16: Also here we consider the two processes in the NEB, starting with an approach of the hydrogen atom from the absolute minimum (■) to a metastable position of hydrogen (H^* , 0.8 eV) and the subsequent hydrogenation step to C_2H_5 with a total barrier height of 1.3 eV.

$\text{C}_2\text{H}_4 \rightarrow \text{C}_2\text{H}_5$ on Pd_1

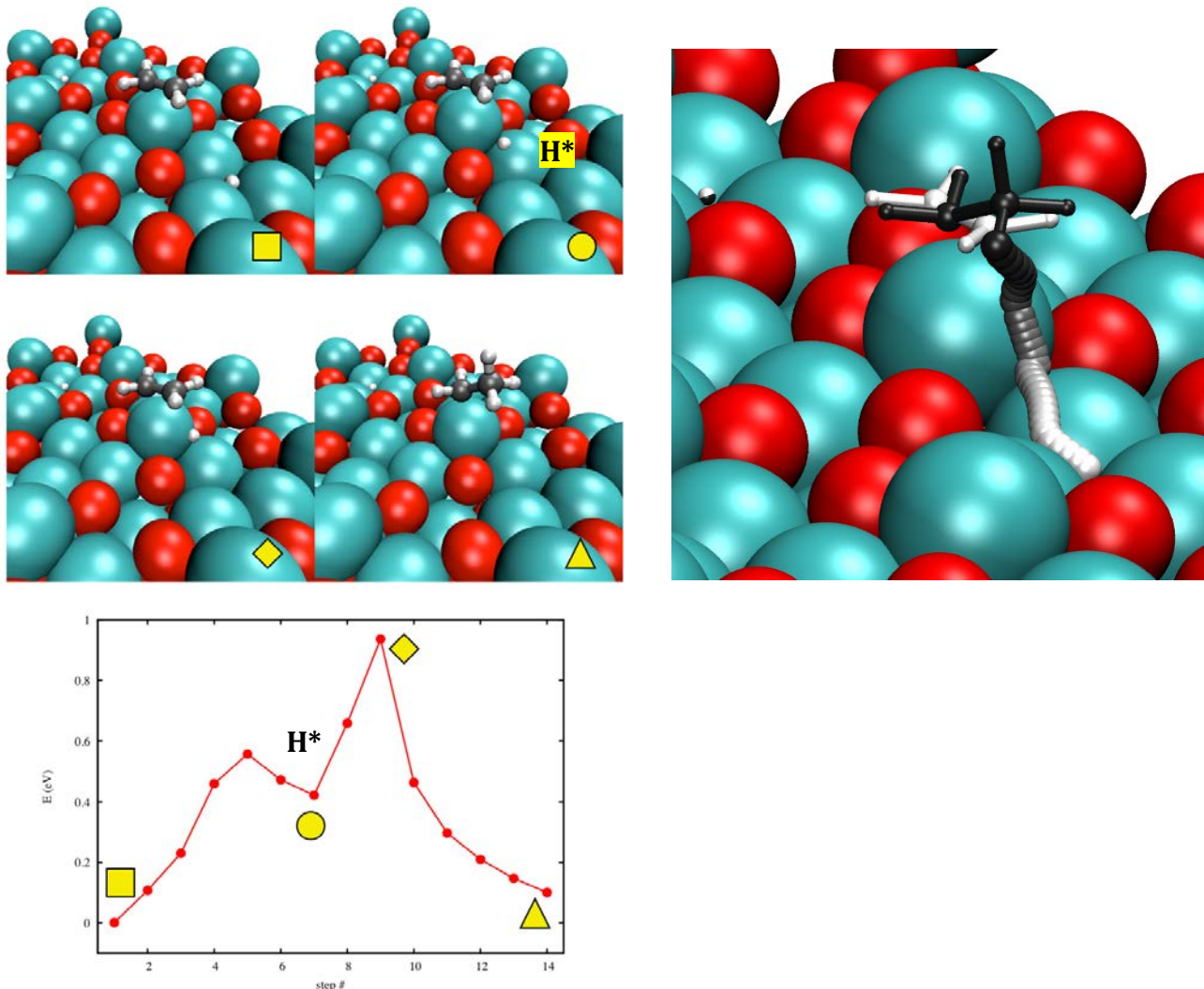


Figure S17: Also for Pd_1 , we include the hydrogen approach in the NEB simulation. The total barrier amounts to 0.9 eV, including the diffusion of H to the metastable position (●) at 0.4 eV, and the subsequent hydrogenation step with a barrier of 0.5 eV. As explained in the manuscript, desorption of ethylene (which has a lower adsorption energy of 0.73 eV) is likely to occur before the barrier for transformation to C_2H_5 is overcome.

References

- (1) Goedecker, S.; Teter, M.; Hutter, J. *Phys. Rev. B* **1996**, *54*, 1703.
- (2) Perdew, J. P.; Burke, K.; Ernzerhof, M. *Phys. Rev. Lett.* **1997**, *78*, 1396.
- (3) Henkelman, G.; Uberuaga, B. P.; Jonsson, H. *Journal of Chemical Physics* **2000**, *113*, 9901.